

Silicon Nanoparticle-Based Ratiometric Fluorescence Probes for Highly Sensitive and Visual Detection of VB₂

Meicheng Lu,[†] Congjie Pan,^{*,†} Xuezhen Qin, and Mingxia Wu^{*}Cite This: *ACS Omega* 2023, 8, 14499–14508

Read Online

ACCESS |



Metrics & More

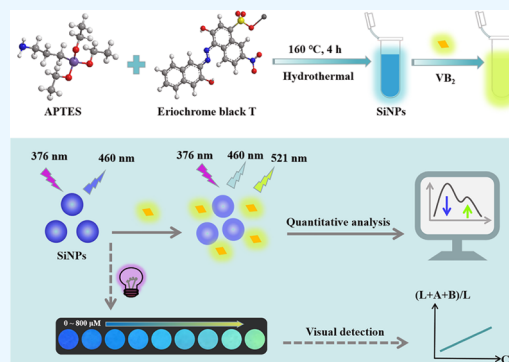


Article Recommendations



Supporting Information

ABSTRACT: In this work, blue fluorescent silicon nanoparticles (SiNPs) were prepared by a simple one-step hydrothermal method using (3-aminopropyl) triethoxy silane (APTES) and eriochrome black T as raw materials. The SiNPs showed favorable water solubility, thermal stability, pH stability, salt tolerance, and photobleaching resistance. At an excitation wavelength of 376 nm, the SiNPs emitted bright blue fluorescence at 460 nm. In the presence of vitamin B₂ (VB₂), the fluorescence intensity (FL intensity) of the SiNPs at 460 nm decreased obviously, and a new peak appeared at 521 nm. Based on this, a novel ratiometric fluorescence method was established for VB₂ detection. There was a good linear relationship between the fluorescence intensity ratio (F_{521}/F_{460}) and VB₂ concentration from 0.5 to 60 μM with a detection limit of 135 nM. This method was successfully applied to detect VB₂ content in the samples of vitamin B₂ drugs and beverages. Additionally, a simple paper sensor based on the SiNPs was designed to visualize detection of VB₂. With the support of color recognition software on a smartphone, the visual quantitative analysis of VB₂ was realized, ranging from 40 to 800 μM .



1. INTRODUCTION

Vitamin B₂ (VB₂), also known as riboflavin, is an essential nutrient for the human body. As the precursor of flavin mononucleotide (FMN) and flavin adenine dinucleotide (FAD), VB₂ plays an important role in energy metabolism and biological oxidation.¹ VB₂ also promotes cell growth and reduces eye strain. Moreover, it can effectively prevent oral inflammation, skin inflammation, migraines, anemia, cancer, and cardiovascular diseases.^{2–5} Since VB₂ cannot be synthesized by the body itself, it needs to be taken from supplements to meet the daily requirement. Most foods are rich in VB₂ such as animal liver, kidney, heart, soy, and dairy products. Besides, as a water-soluble vitamin, VB₂ is not easy to store in the body.⁶ The lack of VB₂ in daily life can cause diseases such as sun sensitivity, glossitis, and seborrheic dermatitis.^{7,8} Additionally, excessive intake of VB₂ can also cause oxidative damage to tissues and DNA, which is also a threat to human health.⁹ In other words, both deficiency and excess of VB₂ are harmful to human health. Therefore, it is of great significance to establish an effective method to detect VB₂.

Common VB₂ detection methods include high-performance liquid chromatography (HPLC),^{10,11} electrochemical,¹² and colorimetric methods.¹³ For example, Geng et al. developed a liquid chromatography–tandem mass spectrometry (LC–MS/MS) method for the detection of vitamins in human serum.¹¹ Wang et al. modified the glassy carbon electrode with nanoporous gold films to achieve the quantitative detection of VB₂ and VB₆.¹² Ma et al. established a riboflavin

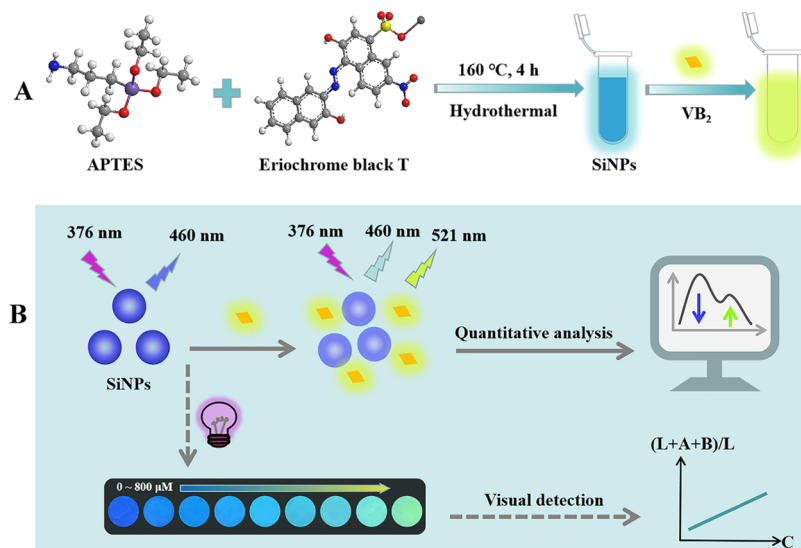
colorimetric sensor based on silver nanoparticles (AgNPs) with a linear range of 0.1667–4.6667 μM .¹³ In recent years, fluorescence methods obtained more and more attention due to their advantages of simple operation, rapid detection, high selectivity, high repeatability, and low cost.^{14–16} Fluorescence methods for detecting VB₂ have also been reported recently. For example, Du et al. utilized dry carnation petals and polyethylene imine as precursors to synthesize carbon dots for detecting VB₂ with a linear range of 0.35–35.9 μM .¹⁷ Wang et al. synthesized carbon quantum dots co-doped with nitrogen, phosphorus, and chlorine (NPCl-CQDs) as a probe to detect VB₂ with detection ranges of 0.5–10.18 and 15.89–27.76 μM .¹⁸ The above methods showed a good response to VB₂ and preliminarily provided a valuable reference for the detection of VB₂. Until now, only a few fluorescence methods for VB₂ detection have been reported. The reported methods still have some shortcomings such as being unfriendly to the environment and a narrow linear range. So, it is still urgent to establish highly sensitive, simple, and environmentally friendly fluorescence methods for VB₂ detection.

Received: January 2, 2023

Accepted: April 5, 2023

Published: April 13, 2023



Scheme 1. Synthesis of the SiNPs (A) and Dual-Platform Detection of VB₂ by Fluorescence and Visualization Methods (B)

Nanomaterials are hyperfine particles with unique optical and physical properties, which are widely used in the fields of biological detection, biosensing, energy storage, etc.^{19,20} Water-soluble fluorescent silicon nanoparticles (SiNPs) are typical zero-dimensional nanomaterials with small-size structure characteristics, visible properties, and phenomena different from macroscopic substances, such as surface effects, quantum size effects, and small-size effects. SiNPs usually have excellent thermal stability, salt resistance, and photobleaching resistance, which is a solid foundation for SiNPs to be excellent fluorescent nanoprobes. There are various one-step methods for preparing water-soluble SiNPs, including electrochemical etching methods,²¹ microwave-assisted methods,²² ultraviolet radiation methods,²³ hydrothermal methods,^{24,25} and so on. Among them, hydrothermal methods are favored by researchers because of their outstanding advantages of mild experimental conditions, cheap equipment, and environmental friendliness. Some researchers found that SiNPs could be completely metabolized by the kidney through pharmacokinetic experiments.²⁶ Green synthesis methods, sufficient silicon raw materials, and environmentally friendly properties are necessary conditions for the long-term development of SiNPs. As novel fluorescent probes, SiNPs have attracted the interest of researchers. In recent years, SiNPs have been used to detect metal ions such as Cu²⁺, Ag⁺, Fe³⁺, Hg²⁺, and Mn²⁺;^{27–30} tetracycline antibiotic drugs such as tetracycline and oxy-tetracycline;^{31,32} and essential nutrients for human body like vitamins, amino acids, glucose, and cholesterol.^{33–36} SiNPs with excellent biocompatibility have also been successfully applied in cell imaging and cell tracking.^{37,38} The above reports indicated that SiNPs have excellent application potential in the field of analytical detection. So far, the fluorescence method based on SiNPs for VB₂ detection has not been reported. Therefore, it is feasible and meaningful to construct a ratiometric fluorescence probe based on SiNPs for VB₂ detection.

In this work, (3-aminopropyl) triethoxy silane (APTES) and eriochrome black T were used as the silicon source and the reducing agent to synthesize SiNPs with blue fluorescence by a hydrothermal method (Scheme 1A). The prepared SiNPs possessed good thermal stability, pH stability, salt tolerance,

and photobleaching resistance. When VB₂ was added to the SiNP solution, the emission peak at 460 nm weakened and, in the meantime, the emission peak at 521 nm enhanced gradually (Scheme 1B). Therefore, a novel ratiometric fluorescence method based on the prepared SiNPs was established for VB₂ detection. The method has been successfully applied to detect VB₂ in the samples of vitamin B₂ tablets, vitamin B₂ injection, compound vitamin B injection, milk, and orange beverage. More importantly, the fluorescence color of the SiNP solution changed from blue to yellow-green with the addition of VB₂. Hence, a visual quantitative detection method for VB₂ detection was established based on a SiNP-fluorescent paper sensor and smartphone (Scheme 1B), which had the advantages of low cost and convenient visualization detection.

2. EXPERIMENTAL SECTIONS

2.1. Synthesis of the SiNPs. First, 4.0 mL of ultrapure water and 1.0 mL of APTES were successively added to a 10 mL round-bottomed flask and placed on a magnetic stirrer for continuous stirring. Then, 5.0 mg of eriochrome black T was added to the above solution. After stirring for 30 min, the mixture solution was transferred to a Teflon-lined reactor. Finally, the reaction was carried out at 160 °C for 4 h. After the reaction, the prepared SiNP solution was dialyzed in a dialysis bag with a molecular weight cutoff of 1000 Da. The obtained SiNP solution was stored in a refrigerator at 4 °C for later use. The purified SiNP solution was lyophilized in a freeze dryer, which could be used for subsequent characterization.

2.2. Fluorescence Detection of VB₂. First, VB₂ was dissolved in HCl solution (5 M) to prepare a 10 mM VB₂ stock solution. Then, the stock solution was diluted with PBS buffer solution (pH 5.0, 10 mM) to prepare a series of VB₂ solutions with different concentrations. One hundred microliters of SiNP solution was mixed with PBS buffer solution (pH 5.0, 10 mM). Afterward, different concentrations of the VB₂ solution were added (the total volume of the solution was 2 mL). After incubation for 1 min, the fluorescence emission spectra of the mixture solution were recorded (the excitation wavelength was 376 nm). Each measurement was repeated three times. The working curve was plotted from the log ($F_{521}/$

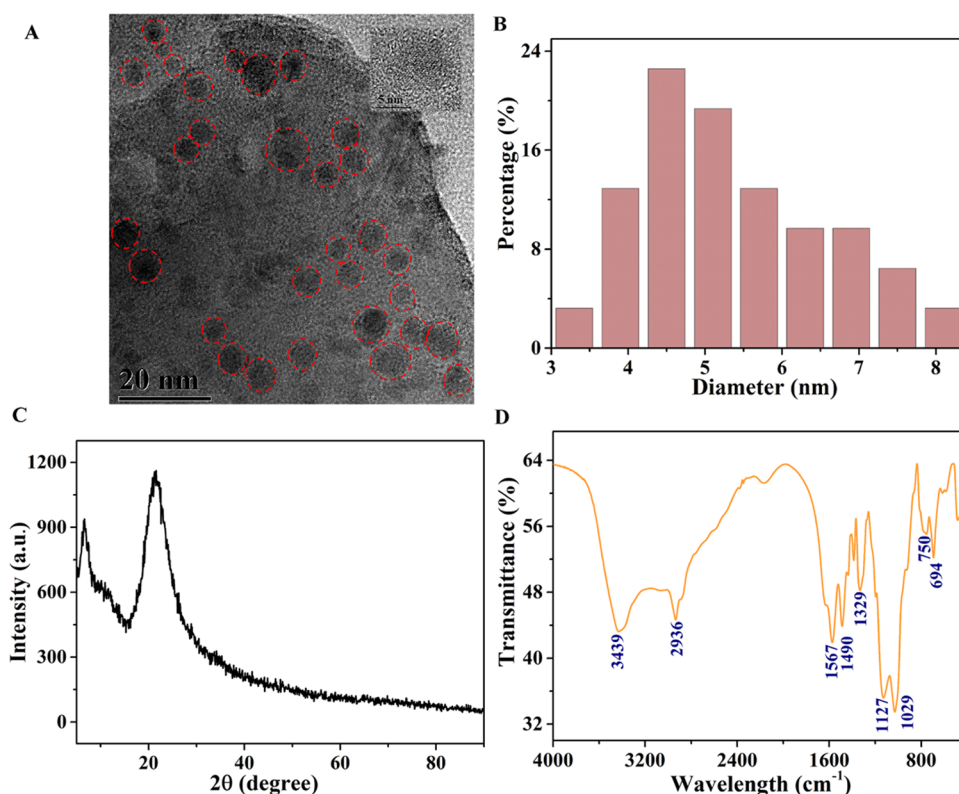


Figure 1. (A) TEM image, (B) corresponding size distribution histogram, (C) PXRD spectrum, and (D) FT-IR spectrum of the SiNPs.

F_{460}) value and VB₂ concentration (F_{460} and F_{521} are the FL intensities of the emission peaks at 460 and 521 nm, respectively).

2.3. Analysis of VB₂ in Real Samples. To evaluate the utility of SiNPs, vitamin B₂ tablets, vitamin B₂ injection, compound vitamin B injection, milk, and orange beverage were selected as real samples. The pretreatment process of the above samples is as follows: ten vitamin B₂ tablets ($m = 0.7783$ g) were ground into powder in a mortar, dissolved in 6.0 mL HCl solution (1 M) to prepare a sample solution, and then centrifuged at 15,000 rpm for 10 min to remove insoluble substances. Finally, the supernatant was collected for detection. Vitamin B₂ injection and compound vitamin B injection were centrifuged at 15,000 rpm for 10 min. The orange beverage was centrifuged at 8000 rpm for 10 min. Then, the supernatant was passed through a 0.22 μ m filter membrane. Four milliliters of milk was diluted with 26 mL of ultrapure water; then, 3 mL of ethanol, 3 mL of 1% potassium oxalate, and 1 mL of 20% zinc acetate solution were added to destroy the fat structure of the milk and precipitate the protein. After precipitation, the precipitation was filtered with filter paper and the extraction solution was collected. These pretreated sample solutions were diluted to an appropriate concentration with PBS buffer solution (10 mM, pH 5.0) for analysis. The fluorescence emission spectra of the above samples were measured at 376 nm excitation. The measured FL intensity ratio (F_{521}/F_{460}) was taken into the linear equation to calculate the VB₂ content of the samples. In addition, known amounts of the VB₂ solution were added to the diluted sample solution for the recovery experiment.

2.4. Preparation of Fluorescent Test Papers and Visual Detection of VB₂. Four milliliters of SiNP solution was added to 16.0 mL of ethanol solution. The filter paper was

put into the above solution and immersed for 2 min. After that, the filter paper was removed from the solution. After natural drying, it was cut to an appropriate size and flattened. Then, 30 μ L of VB₂ solution of different concentrations was added to the prepared test papers. After the test papers were naturally dried, photos were taken under 365 nm UV light. The values of L , A , and B of the fluorescent images were read by color recognition software on a smartphone. Each photo in the dark environment was taken at the same distance and angle. To ensure the accuracy of the experimental results, nine sites were selected in three different regions of the central region, the edge region, and the regions between the center and the edge of each photo to read the corresponding L , A , and B values. Finally, the average value was taken to draw a linear plot. The working curve of $(L + A + B)/L$ and the concentration of VB₂ was drawn to establish the visual detection method of VB₂.

3. RESULTS AND DISCUSSION

3.1. Optimization of Synthesis Conditions for the SiNPs.

To obtain the optimum synthesis condition of the SiNPs, the reaction temperature, reaction time, and the amount of reducing agent were investigated when the volume of APTES was 1.0 mL. As shown in Figure S1A, the FL intensity reached the maximum when the reaction was performed at 160 °C. As shown in Figure S1B, the FL intensity was significantly enhanced when the mass of eriochrome black T increased from 2.5 to 5.0 mg. When the mass of eriochrome black T was up to 15.0 mg, the FL intensity was significantly reduced. As shown in Figure S1C, the FL intensities of the reaction products for 4 h were significantly higher than those for 2 and 8 h. In summary, when APTES and eriochrome black T were used as raw materials to synthesize SiNPs, the optimal conditions of eriochrome black

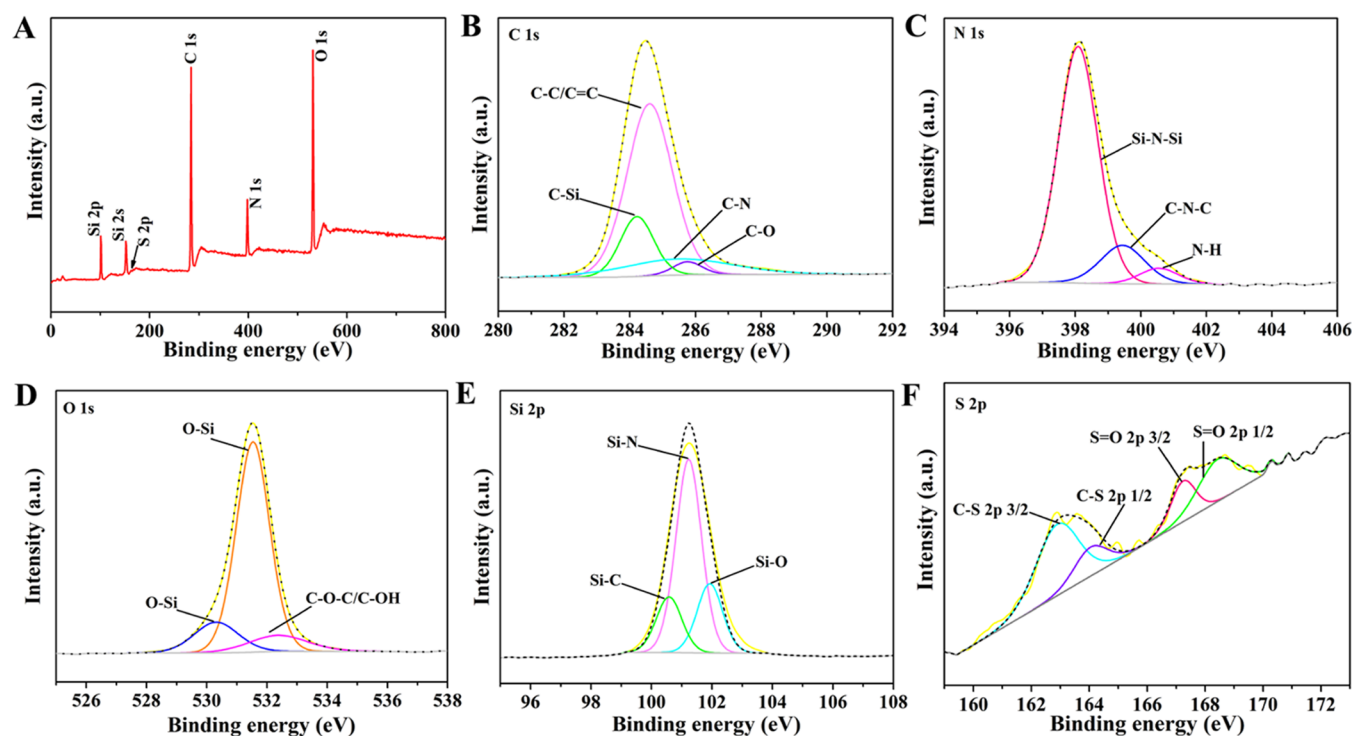


Figure 2. High-resolution XPS spectra of the SiNPs: (A) full spectrum, (B) C 1s, (C) N 1s, (D) O 1s, (E) Si 2p, and (F) S 2p.

T amount, reaction time, and temperature were 5.0 mg, 4 h, and 160 °C, respectively.

As shown in Figure S1D, when the reaction followed the steps described above to prepare SiNPs, the FL intensities of eriochrome black T and APTES reacted alone were very low and negligible. Only when APTES and eriochrome black T reacted together, the FL intensity increased significantly, indicating that a fluorescent substance was generated.

3.2. Characterization of the SiNPs. Transmission electron microscopy (TEM) was used to characterize the morphology of the SiNPs. As shown in Figure 1A, the SiNPs were irregular spherical particles with good dispersion. The particle size of the SiNPs ranged from 3.41 to 8.35 nm, with an average diameter of around 5.35 nm (Figure 1B). X-ray powder diffraction (PXRD) results displayed that the structure of the SiNPs was amorphous (Figure 1C). Figure 1D shows the Fourier transform infrared (FT-IR) spectra of the SiNPs, in which the medium-strong absorption band at 3439 cm^{-1} was the stretching vibration of the N–H bond and O–H bond.³⁹ The absorption band at 2936 cm^{-1} was the stretching vibration of the C–H bond.⁴⁰ The absorption bands at 1567 and 1490 cm^{-1} were the stretching vibrations of the aromatic ring.⁴¹ The absorption band at 1329 cm^{-1} was attributed to the stretching vibration of the C–N bond.⁴⁰ The absorption peak at 1127 cm^{-1} was the stretching vibration of the Si–O–Si bond.⁴⁰ The vibration peak of the Si–C bond was 1029 cm^{-1} .⁴² The absorption bands at 750 and 694 cm^{-1} were the wagging vibration of the N–H bond and the characteristic absorption peaks of the ammonium bond, respectively.⁴⁰ The results of FT-IR suggested that –OH and –NH₂ may exist on the surface of the SiNPs. In addition, X-ray photoelectron spectroscopy (XPS) was used to further analyze the elemental composition and bonding state of the SiNPs. Figure 2A shows the six main peaks of the full spectrum of the SiNPs attributed to Si 2p (101.48 eV), Si 2s (152.48 eV), S 2p (163.13 eV), C

1s (305.48 eV), N 1s (398.48 eV), and O 1s (531.48 eV). The high-resolution XPS spectrum of C 1s (Figure 2B) included four fitting peaks, which belonged to C–C (284.60 eV), C–O (285.75 eV), C–Si (284.22 eV), and C–N (285.48 eV).⁴⁰ The high-resolution XPS spectrum of N 1s (Figure 2C) included three fitting peaks, which belonged to Si–N–Si (398.09 eV), C–N–C (399.44 eV), and N–H (400.55 eV).^{43,44} Three fitted peaks of the high-resolution XPS spectrum of O 1s (Figure 2D) were assigned to O–Si (531.40 eV), O–Si (530.32 eV), and C–O–C/C–OH (532.37 eV).⁴⁵ Three fitting peaks of the high-resolution XPS spectrum of Si 2p (Figure 2E) were attributed to Si–N (101.23 eV), Si–O (101.93 eV), and Si–C (100.58 eV).⁴³ The high-resolution XPS spectrum of S 2p (Figure 2F) presented four fitting peaks, which were assigned to S 2p_{3/2} C–S (162.89 eV), S 2p_{1/2} C–S (164.04 eV), S 2p_{3/2} S=O (167.24 eV), and S 2p_{3/2} S=O (168.43 eV).⁴⁶

The optical properties of the SiNPs were analyzed by ultraviolet–visible (UV–vis) and fluorescence spectra. As seen in Figure S2, the UV–vis spectra showed two characteristic absorption peaks at 239 and 340 nm, which could be attributed to the π – π^* transition and n – π^* transition, respectively.^{47,48} When the excitation wavelength was 376 nm, the FL intensity of the SiNPs reached the strongest at 460 nm. Figure S3A shows the fluorescence emission spectra of the SiNPs at different excitation wavelengths of 310–430 nm. When the excitation wavelength was changed, the fluorescence emission wavelength also changed, indicating that the SiNPs were excitation wavelength-dependent. Excitation wavelength dependence was thought to be caused by the different sizes and surface states of nanoparticles.⁴⁹ Figure S3B shows that the variation range of the fluorescence emission wavelength was small, which demonstrated that the size of the prepared SiNPs was relatively consistent. The relative fluorescence quantum yield of the SiNPs was calculated to be 4.98% (Figure S4 and

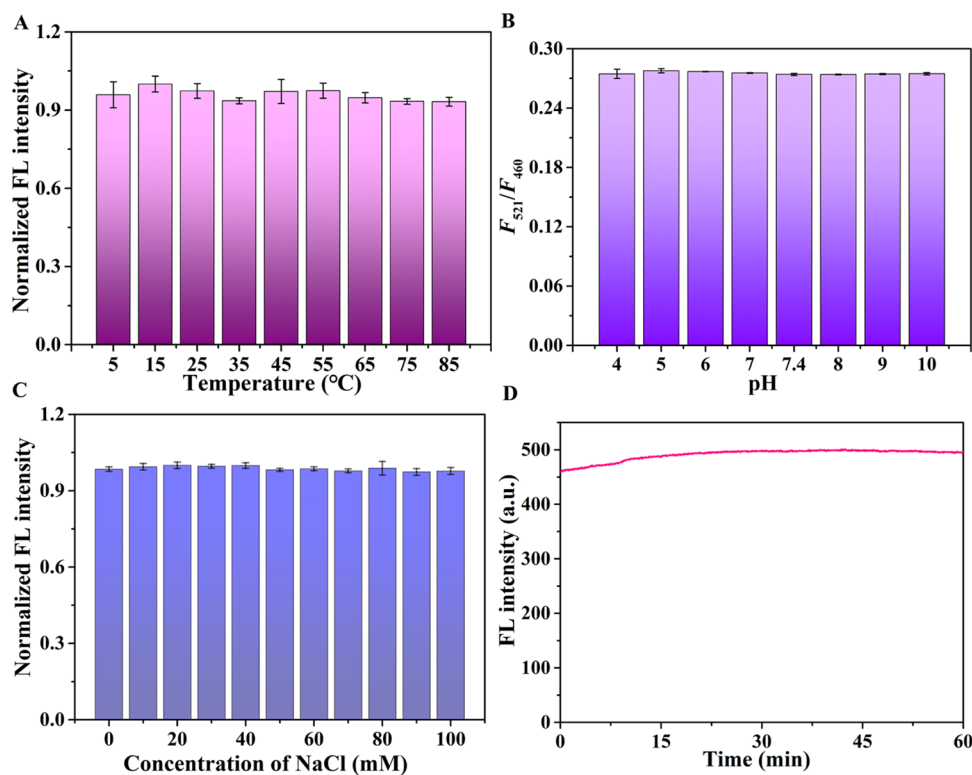


Figure 3. (A) Normalized FL intensity of the SiNPs after 10 min incubation at different temperatures. (B) FL intensity ratio (F_{521}/F_{460}) of the SiNPs in PBS buffer solution (10 mM) of different pH values. (C) Normalized FL intensity of the SiNPs in NaCl solution with different concentrations. (D) FL intensity of the SiNPs exposed to a 376 nm light source for 60 min (the error bar is the standard deviation of three measurements).

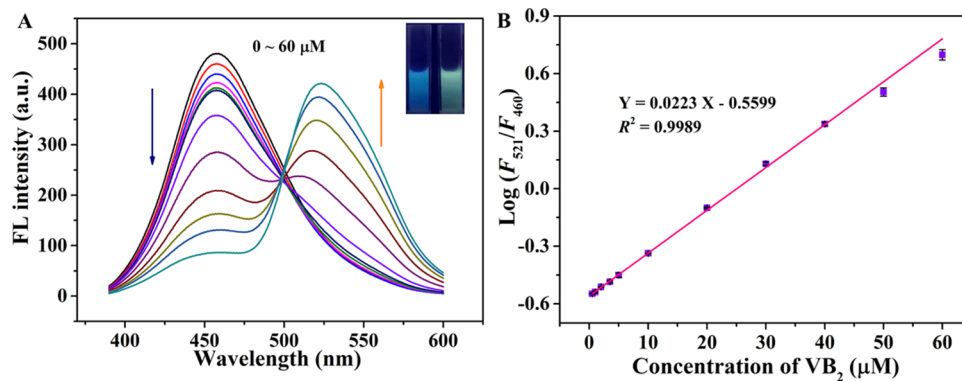


Figure 4. (A) Fluorescence emission spectra of the SiNP solution after addition of different concentrations of VB₂ (0, 0.5, 1, 2, 3.5, 5, 10, 20, 30, 40, 50, and 60 μM); the inset shows the SiNP solution without (left) and with (right) VB₂ under 365 nm UV light. (B) Linear relationship between $\text{log}(F_{521}/F_{460})$ of the SiNPs and 0.5–60 μM VB₂.

Table S1). The excellent fluorescence properties of the SiNPs may be related to the rigid plane introduced by reducing agent eriochrome black T.⁵⁰

3.3. Stability of the SiNPs. In this work, the stability of the SiNPs was investigated by studying the changes of the FL intensity of the SiNPs under different conditions. As shown in Figure 3A–C, when the temperature increased from 5 to 85 °C, the pH increased from 4.0 to 10.0, and when the NaCl concentration was as high as 100 mM, the FL intensity of the SiNPs remained basically unchanged. As can be seen from Figure 3D, when the SiNPs were continuously irradiated by the light source ($\lambda_{\text{ex}} = 376$ nm) for 60 min, the change of FL intensity was negligible. These results showed the excellent

thermal stability, pH stability, salt tolerance, and photo-bleaching resistance of the SiNPs.

3.4. Optimization of VB₂ Detection Conditions. To obtain the optimum detection results and improve the sensitivity of detection, the pH of the PBS buffer solution and response time in the detection process were investigated. As shown in Figure S5A, the FL intensity ratio (F_{521}/F_{460}) of SiNPs remained stable in the PBS buffer solution (10 mM) with pH 4.0–10.0. The pH stability of SiNPs may be due to the fact that the protonation or deprotonation of the functional groups on the surface of SiNPs under different pH conditions did not cause obvious changes in the surface state. After addition of the quencher (VB₂), it was found that VB₂ had the highest response efficiency in the buffer solution with pH 5.0.

Table 1. Comparison of VB₂ Detection Methods

applied material	method	linear range	LOD	ref
	LC–MS/MS	5–40 ng/mL		11
NPG	electrochemical	5–250 μM	0.10 μM	12
AgNPs	colorimetric	0.1667–4.6667 μM	167 nM	13
CDs	fluorescence	0.35–35.9 μM	37.20 nM	17
NPCI-CQDs	fluorescence	0.5–10.18 and 15.89–27.76 μM	3.50 nM	18
NPCDs	fluorescence	0.5–50 μM	0.17 μM	51
SiNPs	fluorescence	0.5–60 μM	135 nM	this work

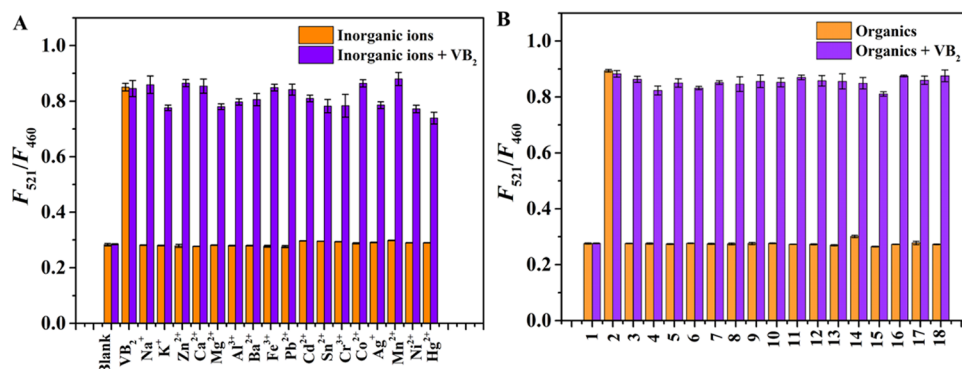


Figure 5. (A) FL intensity ratio (F_{521}/F_{460}) of the SiNPs after addition of 200 μM (the concentration of Cd²⁺, Sn²⁺, Cr³⁺, Co²⁺, Ag⁺, Mn²⁺, Ni²⁺, and Hg²⁺ was 50 μM) inorganic ions (orange bar) and the subsequent addition of 20 μM VB₂ (purple bar). (B) FL intensity ratio (F_{521}/F_{460}) of the SiNPs after addition of 200 μM organic substances (the concentration of VB₉ and VB₁₂ was 100 μM) and the subsequent addition of 20 μM VB₂ (1, blank; 2, VB₉; 3, Gly; 4, Ala; 5, L-Cys; 6, L-Glu; 7, L-Ser; 8, Val; 9, VC; 10, VB₁; 11, VB₃; 12, dextrorphanthenate sodium salts; 13, VB₆; 14, VB₉; 15, VB₁₂; 16, nicotinamide; 17, soluble starch; 18, sucrose).

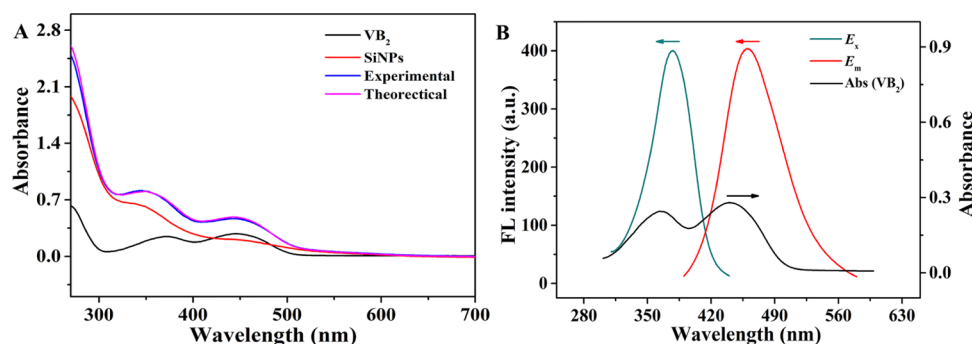


Figure 6. (A) UV–vis spectra of the SiNPs and VB₂ and the theoretical and experimental UV–vis spectra of the mixture of SiNPs and VB₂. (B) UV–vis spectra of VB₂ and the fluorescence excitation and emission spectra of the SiNPs.

Therefore, the optimal pH of the PBS buffer solution in this experiment was 5.0. As seen in Figure S5B, SiNPs and VB₂ (50 μM) reacted rapidly. The reaction reached stability within 1 min. In summary, PBS buffer solution with pH 5.0 and 1 min response time were selected as the optimum detection conditions in the following experiment.

3.5. Fluorescence Detection of VB₂. As shown in Figure 4A, with the increase of VB₂ concentration, the FL intensity of the SiNPs at 460 nm decreased continuously, while the FL intensity of the emission peak at 521 nm increased continuously. The new peak was consistent with the emission peak of VB₂ excited at 376 nm (Figure S6). Figure 4B shows a good linear relationship between $\log(F_{521}/F_{460})$ and VB₂ concentration (0.5–60 μM) with a limit of detection (LOD) of 135 nM ($3\sigma/K$, where σ is the standard deviation of ten blank solutions and K is the slope of the linear equation). Compared with the VB₂ self-fluorescence detection method, the proposed method had higher sensitivity and a wider linear

range (Figure S7). The LOD and linear range of this method were comparable to the VB₂ detection methods listed in Table 1.^{11–13,17,18,51} In addition, the established method also exhibited the following advantages: (1) the preparation process of the SiNPs was simple, environmentally friendly, and did not require postmodification processes; (2) the ratiometric fluorescence method could effectively eliminate the influence of common factors and improve the accuracy of detection; and (3) the paper sensor provided a convenient visual detection platform for VB₂ detection without expensive equipment.

3.6. Selectivity of the SiNPs for VB₂. In this work, some common cations (K⁺, Na⁺, Zn²⁺, Ca²⁺, Mg²⁺, Al³⁺, Ba²⁺, Fe³⁺, Pb²⁺, Cd²⁺, Sn²⁺, Cr³⁺, Co²⁺, Ag⁺, Mn²⁺, Ni²⁺, and Hg²⁺), organic molecules (Gly, Ala, L-Cys, L-Glu, L-Ser, Val, starch, and sucrose), and vitamin drugs (nicotinamide, VC, VB₁, VB₃, dextrorphanthenate sodium salts, VB₆, VB₉, and VB₁₂) were used as potential interference substances to investigate the selectivity of SiNPs for VB₂. Fluorescence detection of the

above interferences was carried out according to the method of VB₂ detection. Figure 5 shows that these interferences did not significantly quench the FL intensity of the SiNPs, which indicated that the SiNPs have superior selectivity for VB₂. In addition, interferences and VB₂ were added to the SiNP solution simultaneously to study the anti-interference ability of the established fluorescence method. The FL intensity of the SiNP solution with only VB₂ and the SiNP solution with both VB₂ and interferences did not change significantly, which indicated that the SiNPs have good anti-interference ability. The above results provided a basis for the detection of VB₂ in practical samples.

3.7. Fluorescence Detection Mechanism of VB₂ by the SiNPs. The fluorescence detection mechanism in this work was studied through the following experiment.

First, the UV–vis spectra of the SiNP solution, VB₂ solution, and their mixture were measured. As shown in Figure 6A, the theoretical UV–vis curve of the mixture solution basically coincided with the experimental UV–vis curve, indicating that no new substances were generated. Subsequently, the excitation and emission spectra of the SiNPs were measured. It was discovered that the UV–vis spectra of VB₂ partially overlapped with both the excitation and emission spectra of the SiNPs (Figure 6B), which speculated that the quenching mechanism of the system may be the internal filtration effect (IFE) and Förster resonance energy transfer (FRET). To further validate the above speculation, the following experiments were conducted. First, the existence of the IFE mechanism was verified by fluorescence and UV–vis spectra of the SiNP solution with different concentrations of VB₂. The correction factor (CF) was calculated by eq 1 to correct the detected FL intensity, which was used to calculate the IFE proportion later. Figure S8 shows the parameters related to eq 1.³⁹ The proportion of IFE calculated based on the values in Table S2 was 48.38% (to ensure the reliability of the calculation results, the CF value cannot be greater than 3).³⁹

$$\frac{F_{\text{cor}}}{F_{\text{obsd}}} = \frac{2.3dA_{\text{ex}}}{1 - 10^{-dA_{\text{ex}}}} 10^{gA_{\text{em}}} \frac{2.3sA_{\text{em}}}{1 - 10^{-sA_{\text{em}}}} \quad (1)$$

Then, the mechanism of FRET was also studied. FRET is a fluorescence quenching process that occurs between the donor and the acceptor. Resonance dipole occurs when the emission spectra of the donor and the absorption spectra of the acceptor partially overlap, and the acceptor produces fluorescence under excitation conditions of the donor. The efficiency of energy transfer depends largely on the degree of the overlap between the emission spectra of the donor (SiNPs) and the UV–vis spectra of the acceptor (VB₂).¹⁷ Moreover, the fluorescence lifetime (τ) of the donor is significantly reduced in the presence of FRET. Figure S9 shows the spectra of the fluorescence decay curves of the SiNPs and SiNPs mixed with different concentrations of VB₂. The τ values in Table S3 were calculated by fitting the fluorescence decay curves with second-order exponential decay. With the increase of VB₂ concentration, the fluorescence lifetime of the SiNPs decreased significantly from 10.89 to 7.34 ns, which further proved the existence of the FRET mechanism.

Additionally, the Stern–Volmer equation (eq 2)⁵² was used to study the dynamic quenching effect (DQE) and static quenching effect (SQE) in the system.

$$F_{\text{cor},0}/F_{\text{cor}} = 1 + K_{\text{sv}}[Q] \quad (2)$$

where $F_{\text{cor},0}$ and F_{cor} are the corrected FL intensities of the SiNPs solution without and with VB₂, respectively. K_{sv} is the Stern–Volmer constant. $[Q]$ is the concentration of VB₂. It can be seen from Figure S10 that $F_{\text{cor},0}/F_{\text{cor}}$ was not linearly related to the concentration of VB₂, indicating that there were no SQE and DQE in the system.

In conclusion, the mechanism of VB₂ detection by the fluorescent SiNPs was IFE and FRET.

3.8. Analysis of VB₂ in Real Samples. To explore the practicability of the established fluorescence method, the VB₂ contents in vitamin B₂ tablets, vitamin B₂ injection, compound vitamin B injection, orange beverage, and milk were detected, respectively. After calculations, the VB₂ contents of vitamin B₂ tablets, vitamin B₂ injection, and compound vitamin B injection were 66.49 mg/g, 5.98 mg/mL, and 1.40 mg/mL, respectively. VB₂ was not detected in the orange beverage and milk based on this method. As shown in Table 2, the recoveries

Table 2. Results of the Detection of VB₂ in Real Samples

sample	initial VB ₂ content (μM)	spiked (μM)	found (μM)	recovery (%)	RSD (%), $n = 3$
vitamin B ₂ tablets	4.44	10.00	14.09 ± 0.04	96.58	0.39
		20.00	23.70 ± 0.68	96.30	3.52
		40.00	42.00 ± 0.15	93.90	0.40
vitamin B ₂ injection	9.93	10.00	20.45 ± 0.15	105.19	1.46
		20.00	30.62 ± 0.19	103.43	0.91
		40.00	49.78 ± 0.61	99.62	1.53
compound vitamin B injection	9.32	10.00	19.08 ± 0.08	97.62	0.83
		20.00	28.31 ± 0.27	94.93	1.45
		40.00	46.39 ± 0.78	92.67	2.10
orange beverage	nd ^a	10.00	9.76 ± 0.18	97.56	1.88
		20.00	18.88 ± 0.54	94.40	2.87
		40.00	36.35 ± 0.21	90.86	0.58
milk	nd ^a	10.00	10.25 ± 0.03	102.50	2.93
		20.00	20.11 ± 0.02	100.57	1.84
		40.00	36.57 ± 0.01	91.43	1.21

^aNot detected.

were in the range of 90.86–105.19%, with relative standard deviations (RSDs) of 0.39–3.52%. These results showed the application prospect of the proposed fluorescence method in practical sample determination.

3.9. Visual Detection of VB₂. In this work, a portable, economical, and rapid detection method for VB₂ visual detection was established using a SiNP-based paper sensor. As shown in Figure 7, the paper sensor showed blue fluorescence under a 365 nm UV lamp. As the concentration of VB₂ increased, the fluorescence color of the paper sensor gradually changed from blue to yellow-green. The fluorescence color of the picture could be identified by color recognition software, and the values of L, A, and B were read. Finally, a linear equation was established according to the value of $(L + A + B)/L$ and the concentration of VB₂. The linear range and LOD were 40–800 and 28.00 μM , respectively. The developed SiNP-based paper sensor was simple, cheap, and had good significance in visual detection of VB₂. Reproducibility was an important factor in the evaluation of the method. The reproducibility was investigated by parallel measurements of test papers containing different concentrations of VB₂ (the VB₂ concentrations were 200, 400, and 600 μM). The RSDs of three parallel measurements were less than 5% (RSDs were

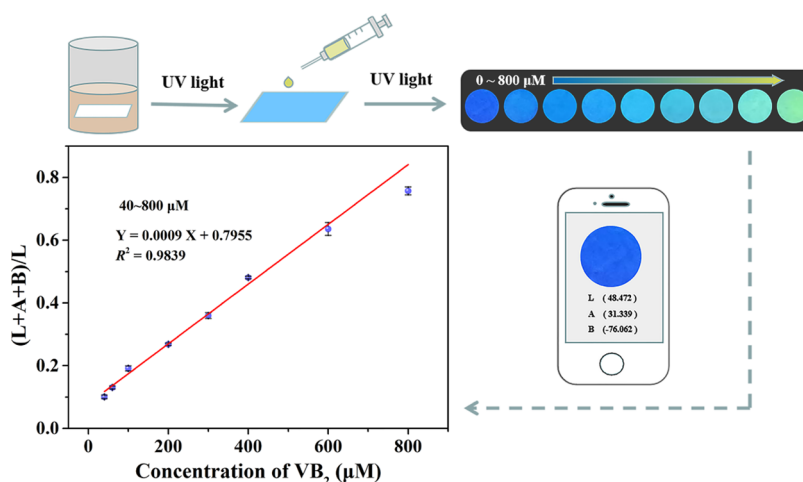


Figure 7. Process of visual detection of VB_2 .

1.45, 0.87, and 3.25%), indicating the good reproducibility of the developed paper sensor. In addition, the paper sensor was used to detect the VB_2 content in the real samples of VB_2 injection and milk. The recoveries were in the range of 86.68–107.36%, and the RSDs were 1.06–6.21% (Table S4).

4. CONCLUSIONS

In summary, the blue fluorescent SiNPs were prepared by a hydrothermal reaction of APTES and eriochrome black T. The synthesis process of the SiNPs was simple, green, low-cost, and did not require complex modification processes. Moreover, the synthesized SiNPs had good thermal stability, pH stability, salt tolerance, and photobleaching resistance. Based on the IFE and FRET mechanisms, the quantitative detection of VB_2 by the SiNPs could be realized. In the meantime, satisfactory results were also obtained in the analysis of samples of vitamin B_2 drugs and beverages. The recoveries were in the range of 90.86–105.19%. In addition, the SiNPs were also successfully utilized for the visual quantitative detection of VB_2 using a smartphone as a portable tool. The SiNP-based paper sensor provided a convenient and economical visual detection method for VB_2 detection without expensive equipment. Nonetheless, it is worth noting that the detection method designed in this experiment also has some limitations. The sensitivity of this method still needs to be further improved. Additionally, the fluorescence color of the ratiometric fluorescence method changed from blue to yellow-green. The change in the color of fluorescent probes from blue to longer-wavelength orange-red should be considered in the later design of the experiment.

■ ASSOCIATED CONTENT

SI Supporting Information

The Supporting Information is available free of charge at <https://pubs.acs.org/doi/10.1021/acsomega.3c00025>.

Reagents and instruments used in the experiment; calculation formula and results of the relative quantum yield of the SiNPs; optimization of the SiNP synthesis conditions; UV–vis absorption spectra, optimal excitation, and emission spectra of the SiNPs; fluorescence emission spectra of the SiNPs at different excitation wavelengths; optimization of VB_2 detection conditions; fluorescence emission spectra of VB_2 excited at 376 nm; optimization and establishment of the VB_2 self-

fluorescence method; geometry of the fluorescence measurements; fluorescence decay curves and data; graph of relationship between the SiNPs fluorescence intensity and VB_2 concentration; and calculation of the proportion of IFE (PDF)

■ AUTHOR INFORMATION

Corresponding Authors

Congjie Pan – School of Pharmacy, Henan University of Chinese Medicine, Zhengzhou 450046, China; orcid.org/0000-0002-4896-7195; Email: pancongjie@hactcm.edu.cn

Mingxia Wu – School of Pharmacy, Henan University of Chinese Medicine, Zhengzhou 450046, China; Email: mxwu711@163.com

Authors

Meicheng Lu – School of Pharmacy, Henan University of Chinese Medicine, Zhengzhou 450046, China

Xuezhen Qin – School of Pharmacy, Henan University of Chinese Medicine, Zhengzhou 450046, China

Complete contact information is available at:

<https://pubs.acs.org/10.1021/acsomega.3c00025>

Author Contributions

[†]M.C.L. and C.J.P. contributed equally to this work.

Notes

The authors declare no competing financial interest.

■ ACKNOWLEDGMENTS

The authors are grateful for financial support from the Zhongjing Scholars Research Funding of Henan University of Chinese Medicine (No. 00104311-2022-1-12).

■ REFERENCES

- (1) Zha, Z.; Tang, R.; Wang, C.; Li, Y. L.; Liu, S.; Wang, L.; Wang, K. Riboflavin inhibits browning of fresh-cut apples by repressing phenolic metabolism and enhancing antioxidant system. *Postharvest Biol. Technol.* **2022**, *187*, No. 111867.
- (2) Zou, Y. X.; Ruan, M. H.; Luan, J.; Feng, X.; Chen, S.; Chu, Z. Y. Anti-aging effect of riboflavin via endogenous antioxidant in fruit fly *Drosophila melanogaster*. *J. Nutr., Health Aging* **2017**, *21*, 314–319.
- (3) Saedisomeolia, A.; Ashoori, M. Chapter two-riboflavin in human health: a review of current evidences. *Adv. Food Nutr. Res.* **2018**, *83*, 57–81.

- (4) Yamanaka, G.; Suzuki, S.; Morishita, N.; Takeshita, M.; Kanou, K.; Takamatsu, T.; Morichi, S.; Ishida, Y.; Watanabe, Y.; Go, S.; et al. Experimental and clinical evidence of the effectiveness of riboflavin on migraines. *Nutrients* **2021**, *13*, No. 2612.
- (5) You, J.; Pan, X.; Yang, C.; Du, Y.; Osire, T.; Yang, T.; Zhang, X.; Xu, M.; Xu, G.; Rao, Z. Microbial production of riboflavin: biotechnological advances and perspectives. *Metab. Eng.* **2021**, *68*, 46–58.
- (6) Thakur, K.; Tomar, S. K.; Singh, A. K.; Mandal, S.; Arora, S. Riboflavin and health: a review of recent human research. *Crit. Rev. Food Sci. Nutr.* **2017**, *57*, 3650–3660.
- (7) Pinto, J. T.; Zempleni, J. Riboflavin. *Adv. Nutr.* **2016**, *7*, 973–975.
- (8) Suwannasom, N.; Kao, I.; Pruß, A.; Georgieva, R.; Bäumlner, H. Riboflavin: the health benefits of a forgotten natural vitamin. *Int. J. Mol. Sci.* **2020**, *21*, No. 950.
- (9) Zhou, T.; Li, H.; Shang, M.; Sun, D.; Liu, C.; Che, G. Recent analytical methodologies and analytical trends for riboflavin (vitamin B₂) analysis in food, biological and pharmaceutical samples. *TrAC, Trends Anal. Chem.* **2021**, *143*, No. 116412.
- (10) Schmidt, A.; Schreiner, M. G.; Mayer, H. K. Rapid determination of the various native forms of vitamin B₆ and B₂ in cow's milk using ultra-high performance liquid chromatography. *J. Chromatogr. A* **2017**, *1500*, 89–95.
- (11) Geng, C.; Guo, X.; Liu, J.; Gao, M.; Yuan, G.; Bu, F.; Chen, X.; Wang, B.; Guo, R. LC-MS/MS for the determination of four water-soluble vitamins: method development, validation and comparison to EC method. *Chromatographia* **2017**, *80*, 259–264.
- (12) Wang, H.; Zhang, X.; Wang, S.; Xiao, S.; Ma, H.; Wang, X. Multianalyte electrochemical electrode for the determination of vitamins B₂ and B₆ in complex biosystem. *Microchem. J.* **2020**, *158*, No. 105233.
- (13) Ma, Q.; Song, J.; Zhang, S.; Wang, M.; Guo, Y.; Dong, C. Colorimetric detection of riboflavin by silver nanoparticles capped with β -cyclodextrin-grafted citrate. *Colloids Surf., B* **2016**, *148*, 66–72.
- (14) Zhu, S.; Wang, S.; Xia, M.; Wang, B.; Huang, Y.; Zhang, D.; Zhang, X.; Wang, G. Intracellular imaging of glutathione with MnO₂ nanosheet@Ru(bpy)₃²⁺-UiO-66 nanocomposites. *ACS Appl. Mater. Interfaces* **2019**, *11*, 31693–31699.
- (15) Han, T.; Zhu, S.; Wang, S.; Wang, B.; Zhang, X.; Wang, G. Fluorometric methods for determination of H₂O₂, glucose and cholesterol by using MnO₂ nanosheets modified with 5-carboxy-fluorescein. *Microchim. Acta* **2019**, *186*, No. 269.
- (16) Chen, J.; Han, T.; Feng, X.; Wang, B.; Wang, G. A poly(thymine)-templated fluorescent copper nanoparticle hydrogel-based visual and portable strategy for an organophosphorus pesticide assay. *Analyst* **2019**, *144*, 2423–2429.
- (17) Du, F.; Cheng, Z.; Wang, G.; Li, M.; Lu, W.; Shuang, S.; Dong, C. Carbon nanodots as a multifunctional fluorescent sensing platform for ratiometric determination of vitamin B₂ and “turn-off” detection of pH. *J. Agric. Food Chem.* **2021**, *69*, 2836–2844.
- (18) Wang, Z.; Zhang, L.; Hao, Y.; Dong, W.; Liu, Y.; Song, S.; Shuang, S.; Dong, C.; Gong, X. Ratiometric fluorescent sensors for sequential on-off-on determination of riboflavin, Ag⁺ and L-cysteine based on NPCl-doped carbon quantum dots. *Anal. Chim. Acta* **2021**, *1144*, 1–13.
- (19) Xu, Q.; Niu, Y.; Li, J.; Yang, Z.; Gao, J.; Ding, L.; Ni, H.; Zhu, P.; Liu, Y.; Tang, Y.; et al. Recent progress of quantum dots for energy storage applications. *Carbon Neutrality* **2022**, *1*, No. 13.
- (20) Niu, Y.; Li, J.; Gao, J.; Ouyang, X.; Cai, L.; Xu, Q. Two-dimensional quantum dots for biological applications. *Nano Res.* **2021**, *14*, 3820–3839.
- (21) Pham, V. H.; Hanh, N. T. H.; Tam, P. D. Tunable luminescence of nanoporous silicon via electrochemical etching parameters. *Optik* **2016**, *127*, 3513–3516.
- (22) Zhong, Y.; Song, B.; Shen, X.; Guo, D.; He, Y. Fluorescein sodium ligand-modified silicon nanoparticles produce ultrahigh fluorescence with robust pH- and photo-stability. *Chem. Commun.* **2019**, *55*, 365–368.
- (23) Zhong, Y.; Sun, X.; Wang, S.; Peng, F.; Bao, F.; Su, Y.; Li, Y.; Lee, S. T.; He, Y. Facile, large-quantity synthesis of stable, tunable-color silicon nanoparticles and their application for long-term cellular imaging. *ACS Nano* **2015**, *9*, 5958–5967.
- (24) Pan, C.; Qin, X.; Lu, M.; Ma, Q. Water soluble silicon nanoparticles as a fluorescent probe for highly sensitive detection of rutin. *ACS Omega* **2022**, *7*, 28588–28596.
- (25) Pan, C.; Wen, Q.; Ma, L.; Qin, X.; Feng, S. Novel water-dispersible silicon nanoparticles as a fluorescent and colorimetric dual-mode probe for emodin detection. *New J. Chem.* **2021**, *45*, 12528–12537.
- (26) Ji, X.; Wang, H.; Song, B.; Chu, B.; He, Y. Silicon nanomaterials for biosensing and bioimaging analysis. *Front. Chem.* **2018**, *6*, No. 38.
- (27) Wang, Y.; Tian, M.; Xie, W.; Li, C. M.; Liu, Y. One-step synthesis of amine-functionalized fluorescent silicon nanoparticles for copper(II) ion detection. *Anal. Bioanal. Chem.* **2019**, *411*, 6419–6426.
- (28) Zhu, B.; Ren, G.; Tang, M.; Chai, F.; Qu, F.; Wang, C.; Su, Z. Fluorescent silicon nanoparticles for sensing Hg²⁺ and Ag⁺ as well visualization of latent fingerprints. *Dyes Pigm.* **2018**, *149*, 686–695.
- (29) Adinarayana, T. V. S.; Mishra, A.; Singhal, I.; Reddy, D. V. R. K. Facile green synthesis of silicon nanoparticles from *Equisetum arvense* for fluorescence based detection of Fe(III) ions. *Nanoscale Adv.* **2020**, *2*, 4125–4132.
- (30) Meng, L.; Yuan, Y.; Pu, G.; Xu, N. An “on-off-on” fluorescence assay based on silicon nanoparticles for selective detection of manganese(ii). *Anal. Methods* **2017**, *9*, 2553–2560.
- (31) Lin, B.; Zhang, T.; Xin, X.; Wu, D.; Huang, Y.; Liu, Y.; Cao, Y.; Guo, M.; Yu, Y. Europium(III) modified silicone nanoparticles for ultrasensitive visual determination of tetracyclines by employing a fluorescence color switch. *Microchim. Acta* **2019**, *186*, No. 442.
- (32) Xu, N.; Yuan, Y.; Yin, J. H.; Wang, X.; Meng, L. One-pot hydrothermal synthesis of luminescent silicon-based nanoparticles for highly specific detection of oxytetracycline via ratiometric fluorescent strategy. *RSC Adv.* **2017**, *7*, 48429–48436.
- (33) Lu, Q.; Chen, X.; Liu, D.; Wu, C.; Liu, M.; Li, H.; Zhang, Y.; Yao, S. A turn-on fluorescent probe for vitamin C based on the use of a silicon/CoOOH nanoparticle system. *Microchim. Acta* **2019**, *186*, No. 72.
- (34) Ru, F.; Du, P.; Lu, X. Efficient ratiometric fluorescence probe utilizing silicon particles/gold nanoclusters nanohybrid for “on-off-on” bifunctional detection and cellular imaging of mercury (II) ions and cysteine. *Anal. Chim. Acta* **2020**, *1105*, 139–146.
- (35) Yang, C.; Gao, N.; Liu, Y.; Zhao, H.; Jing, J.; Zhang, X. A silicon nanoparticle-based nanoprobe for ratiometric fluorescence and visual detection of glucose. *New J. Chem.* **2021**, *45*, 19515–19520.
- (36) Ye, X.; Jiang, Y.; Mu, X.; Sun, Y.; Ma, P.; Ren, P.; Song, D. Ultrabright silicon nanoparticle fluorescence probe for sensitive detection of cholesterol in human serum. *Anal. Bioanal. Chem.* **2022**, *414*, 3827–3836.
- (37) Cui, K.; Chang, Y.; Liu, P.; Yang, L.; Liu, T.; Zheng, Z.; Guo, Y.; Ma, X. Cell-tailored silicon nanoparticles with ultrahigh fluorescence and photostability for cellular imaging. *ACS Sustainable Chem. Eng.* **2020**, *8*, 17439–17446.
- (38) Kim, G. H.; Lee, G.; Kang, M. H.; Kim, M.; Jin, Y.; Beck, S.; Cheon, J.; Sung, J.; Joo, J. Luminescent silicon nanoparticles for distinctive tracking of cellular targeting and trafficking. *Faraday Discuss.* **2020**, *222*, 304–317.
- (39) Han, Y.; Chen, Y.; Liu, J.; Niu, X.; Ma, Y.; Ma, S.; Chen, X. Room-temperature synthesis of yellow-emitting fluorescent silicon nanoparticles for sensitive and selective determination of crystal violet in fish tissues. *Sens. Actuators, B* **2018**, *263*, 508–516.
- (40) Nsanamahoro, S.; Wang, W. F.; Zhang, Y.; Shi, Y. P.; Yang, J. L. Synthesis of orange-emissive silicon nanoparticles as “off-on” fluorescence probe for sensitive and selective detection of L-methionine and copper. *Talanta* **2021**, *231*, No. 122369.
- (41) Han, Y.; Wang, Y.; Liu, X.; Chen, J.; Qiu, H. Green- and red-emitting fluorescent silicon nanoparticles: synthesis, mechanism, and acid phosphatase sensing. *ACS Appl. Bio Mater.* **2022**, *5*, 295–304.

(42) Han, Y.; Chen, Y.; Feng, J.; Na, M.; Liu, J.; Ma, Y.; Ma, S.; Chen, X. Investigation of nitrogen content effect in reducing agent to prepare wavelength controllable fluorescent silicon nanoparticles and its application in detection of 2-nitrophenol. *Talanta* **2019**, *194*, 822–829.

(43) Geng, X.; Li, Z.; Hu, Y.; Liu, H.; Sun, Y.; Meng, H.; Wang, Y.; Qu, L.; Lin, Y. One-pot green synthesis of ultrabright N-doped fluorescent silicon nanoparticles for cellular imaging by using ethylenediaminetetraacetic acid disodium salt as an effective reductant. *ACS Appl. Mater. Interfaces* **2018**, *10*, 27979–27986.

(44) Zhang, L.; Chen, J.; Zhang, F.; Xu, J.; Bi, N.; Gou, J.; Jia, L. Silicon quantum dots and MOFs hybrid multicolor fluorescent nanosensor for ultrasensitive and visual intelligent sensing of tetracycline. *Colloids Surf., A* **2022**, *652*, No. 129853.

(45) Nsanzamahoro, S.; Mutuyimana, F. P.; Han, Y.; Ma, S.; Na, M.; Liu, J.; Ma, Y.; Ren, C.; Chen, H.; Chen, X. Highly selective and sensitive detection of catechol by one step synthesized highly fluorescent and water-soluble silicon nanoparticles. *Sens. Actuators, B* **2019**, *281*, 849–856.

(46) Ju, B.; Zhang, T.; Li, S.; Liu, J.; Zhang, W.; Li, M.; Zhang, S. X. A. Fingerprint identification of copper ions with absorption and emission dual-mode responses by N,S co-doped red carbon dots. *New J. Chem.* **2019**, *43*, 168–174.

(47) Mua, Z.; Hua, J.; Yang, Y. N, S, I co-doped carbon dots for folic acid and temperature sensing and applied to cellular imaging. *Spectrochim. Acta, Part A* **2020**, *224*, No. 117444.

(48) Zhan, J.; Peng, R.; Wei, S.; Chen, J.; Peng, X.; Xiao, B. Ethanol-precipitation-assisted highly efficient synthesis of nitrogen-doped carbon quantum dots from chitosan. *ACS Omega* **2019**, *4*, 22574–22580.

(49) Divya, S.; Narayan, S.; Ainavarapu, S. R. K.; Khushalani, D. Insight into the excitation-dependent fluorescence of carbon dots. *ChemPhysChem* **2019**, *20*, 984–990.

(50) Wang, J. F.; Yao, Y.; Ning, Y.; Meng, Y. S.; Hou, C. L.; Zhang, J.; Zhang, J. L. The design of rigid cyclic tripyrrins: the importance of intermolecular interactions on aggregation and luminescence. *Org. Chem. Front.* **2018**, *5*, 1877–1885.

(51) Lin, L.; Wang, Y.; Xiao, Y.; Chen, X. Ratiometric fluorescence detection of riboflavin based on fluorescence resonance energy transfer from nitrogen and phosphorus co-doped carbon dots to riboflavin. *Anal. Bioanal. Chem.* **2019**, *411*, 2803–2808.

(52) Anand, S. R.; Bhati, A.; Saini, D.; Gunture; Chauhan, N.; Khare, P.; Sonkar, S. K. Antibacterial nitrogen-doped carbon dots as a reversible “fluorescent nanoswitch” and fluorescent ink. *ACS Omega* **2019**, *4*, 1581–1591.